Classical Trajectory Study of the Dynamics of the Reaction of Cl Atoms with Ethane†

Stuart J. Greaves and Andrew J. Orr-Ewing*

School of Chemistry, University of Bristol, Bristol BS8 1TS, U.K.

Diego Troya

Department of Chemistry, Virginia Tech, 107 Davidson Hall, Blacksburg, Virginia, 24061-0212

Received: March 18, 2008; Revised Manuscript Received: May 30, 2008

We present an electronic-structure and dynamics study of the $Cl + C_2H_6 \rightarrow HCl + C_2H_5$ reaction. The stationary points of the ground-state potential energy surface have been characterized using various electronic-structure methods and basis sets. Our best calculations, CCSD(T) extrapolated to the complete basis limit, using geometries and harmonic frequencies obtained at the MP2/aug-cc-pVTZ level, are in agreement with the experimental reaction energy. Ab initio information has been used to reparameterize a semiempirical Hamiltonian so that the predictions of the improved Hamiltonian agree with the higher-level calculations in key regions of the potential energy surface. The improved semiempirical Hamiltonian is then used to propagate quasiclassical trajectories. Computed kinetic energy release and scattering angle distributions at a collision energy of ~5.5 kcal mol^{-1} are in reasonable agreement with experiments, but no evidence was found for the low translational energy HCl products scattered in the backward hemisphere reported in recent experiments.

I. Introduction

Reactions of small alkanes with atomic oxygen, fluorine, and chlorine have served as important benchmark systems for experimental investigation of the dynamics of reactions of polyatomic molecules.[1–4] The reactions of Cl atoms with methane (including deuterated isotopologues),[5–12] for example, illustrate the effects of translational and vibrational energy on reaction cross sections, vibrational mode and bond-specific dynamics, nonadiabatic dynamics on coupled potential energy surfaces (PESs), and the consequences of scattering resonances. Advances in theoretical methods are making the generation of fully dimensional PESs and the calculation of quantum scattering dynamics for the methane reactions increasingly tractable, despite the large number of degrees of freedom.[13] Experiments are, however, now extending to the study of dynamics of reactions of halogen atoms with larger alkanes and other classes of organic molecules.[14]

The reaction

$$Cl + C_2H_6 \rightarrow HCl + C_2H_5 \qquad (1)$$

illustrates how experiments have been able to derive distributions of population of HCl molecules over rotational energy levels, angular momentum polarization of reaction products, center-of-mass (COM) frame differential cross sections (DCSs), and kinetic energy release distributions, in some cases with quantum-state resolution.[15–22] The reaction is considered to be direct and to occur over a wide range of impact parameters, with passage through a loosely constrained transition state (TS). The HCl is formed with very low levels of rotational excitation at low collision energies, most likely because of a near-collinear Cl−H−C minimum energy geometry at the TS and nonimpulsive release of energy as the H atom transfers. The C_2H_5 product radical thus acquires only ~22% of the available energy as vibrational and rotational motion, with the balance released as kinetic energy of both products.[20] A recent study, however, reported a bimodal distribution of kinetic energies of the subset of backward scattered HCl products under crossed-molecular-beam conditions. The observation of slow HCl products was attributed to chattering collisions in which rapid motion of the transferred H atom between heavier Cl and C atoms in the vicinity of the transition-state coupled energy into the internal degrees of freedom of the C_2H_5 radical.[21,22]

The large number of participant atoms means that the dynamics of reaction 1 currently remain beyond the scope of ab initio calculation of a global PES and fully dimensional quantum mechanical (QM) scattering methods. Barrier heights and the overall energy change for the reaction have been calculated using a variety of ab initio methods, with the results used to determine the rates of the title reaction.[23,24] The reaction has also been the subject of prior dynamical calculations using the quasi-classical trajectory (QCT) method, but these circumvented the need for a global analytic PES by using on-the-fly calculation of potential energy and gradients along the pathways followed by the propagation of classical trajectories. The calculations either used semiempirical[24,25] or ab initio[26] computational methods, with the latter restricted to Hartree−Fock (HF) or second-order Møller−Plesset (MP2) levels by the expense of propagation of trajectories over a few thousand time (and thus potential energy) steps. We previously computed half-trajectories, initiated from the transition state with Wigner sampling of initial conditions from the vibrational degrees of freedom. These half-trajectories were not capable of generating a complete DCS because of the tightly restricted range of reactive impact parameters. As with all classical trajectories, however, the half-trajectories were able to give valuable mechanistic insights. More recently, we extended such calculations for reaction (1) to start from reagents separated by 4.5 Å.[25] The motivation for that study was to seek evidence for the chattering collision mechanism postulated by Suits and co-workers,[21,22] and we thus employed a restricted range of

* Author to whom correspondence should be addressed. E-mail: A.Orr-Ewing@bristol.ac.uk.

† Part of the "Stephen R. Leone Festschrift".

10.1021/jp802347v CCC: $40.75
Published on Web 07/17/2008

TABLE 1: Energetics of the Cl + C_2H_6 → HCl + C_2H_5 Reaction (in kcal/mol)[a]

	reaction energy	barrier
MP2/aug-cc-pVDZ	−1.60 (3.57)	−1.77 (2.60)
MP2/aug-cc-pVTZ	−2.98 (2.27)	−2.28 (2.04)
CCSD/aug-cc-pVDZ	−0.89 (4.37)	0.56 (4.96)
CCSD(T)/aug-cc-pVDZ	−1.21 (4.02)	−1.43 (2.99)
CCSD(T)/aug-cc-pVDZ//MP2-aug-cc-pVTZ	−1.10 (4.15)	−1.34 (2.98)
CCSD(T)/aug-cc-pVTZ//MP2-aug-cc-pVTZ	−2.13 (3.12)	−1.68 (2.63)
CCSD(T)/aug-cc-pVQZ//MP2-aug-cc-pVTZ	−3.05 (2.20)	−2.31 (2.00)
CCSD(T)/CBS[b]//MP2-aug-cc-pVTZ	−3.71 (1.53)	−2.77 (1.54)
AM1	−25.73 (−20.70)	[c]
PM3	−22.48 (−16.79)	[c]
MSINDO	−14.04 (−8.04)	−0.54 (3.46)
SRP-AM1	−2.58 (2.59)	−1.97 (2.99)
exp (298 K)	−2.08 ± 0.39,[51] −2.11 ± 0.41[27]	0.147 ± 0.026[34]

[a] Values in parentheses correspond to classical values, i.e., not zero-point corrected. All of the calculations are based on unrestricted wave functions. [b] Complete basis-set estimate according to a two-point extrapolation procedure[32] employing single-point energies at the CCSD(T)/aug-cc- pVQZ//MP2-aug-cc-pVTZ and CCSD(T)/aug-cc- pVTZ//MP2-aug-cc-pVTZ levels. [c] AM1 and PM3 gave no first order saddle point.

initial orientations and impact parameters to optimize the likelihood of observing chattering dynamics.

This paper presents findings of the first unrestricted and fully dimensional trajectory study into the title reaction, using an approach to obtain the potential energy function employed in our prior search for chattering dynamics.[25] Our approach first examined critical regions of the PES using high-quality electronic-structure methods. We then used these calculations to improve the description of the global PES by the AM1 semiempirical Hamiltonian via reoptimization of the parameters of this Hamiltonian. We subsequently propagated quasi-classical trajectories using the improved specific reaction parameter (SRP) AM1 Hamiltonian to study the DCS and product energy distributions. Detailed comparisons between the results of the QCT calculations and experiments are presented.

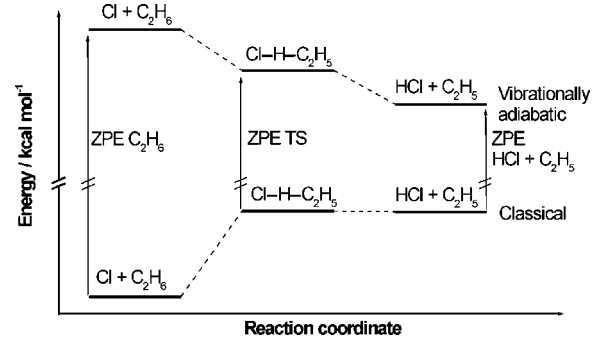

Figure 1. Schematic diagram of the classical and vibrationally adiabatic (i.e., including ZPE) minimum energy paths of reaction 1. The reaction energies correspond to CCSD(T)/CBS//MP2/aug-cc-pVTZ calculations. Pre and post-TS complexes are omitted for clarity. See the text for further details.

II. Ab Initio Study

Reaction (1) is slightly exothermic [−2.1 ± 0.4 kcal mol^{-1} (ref 27)], and the minimum-energy path connecting reagents and products is characterized by a transition state of C_s symmetry, in which the Cl−H bond that forms is nearly collinear with the C−H bond that breaks. High-quality calculations of the reaction energy and barrier using several ab initio methods and basis sets are described in this section. The methods include MP2, coupled-cluster with single and double excitations (CCSD), and perturbative treatment of triple excitations [CCSD(T)], in combination with the augmented double-, triple- and quadruple-ζ correlation-consistent basis sets of Dunning (aug-cc-pVDZ, aug-cc-pVTZ, and aug-cc-pVQZ, respectively).[28,29] The calculations do not include effects of spin−orbit splitting in the Cl atoms and only the valence electrons are correlated. All calculations (ab initio and trajectory) were performed on a Beowulf cluster of 45 networked, dual processor (1.8 GHz, 1 Gb RAM per node) personal computers (PCs). The electronic-structure calculations were conducted with the GAUSSIAN03[30] and MOLPRO[31] programs.

The energetics of the reaction were previously studied computationally by Fernández-Ramos et al.[24] at the lower MP2/aug-cc-pVDZ and MP2/cc-pVTZ levels of theory for geometry optimization, and at the CCSD(T)/IB level (with extrapolation to the infinite basis set limit) for single point energies. Roberto-Neto et al.[23] had earlier examined the reaction using a range of computational methods but did not pursue study of the van der Waals well in the products' valley region.

A. Reaction Energy. The results of our calculations of the energy changes for the reaction and the barrier height are displayed in Table 1, and are compared with experimental data. With the inclusion of zero-point energy (ZPE), the reaction is shown to be slightly exothermic, and the barrier is "submerged" so that it lies at an energy below that of separated Cl and C_2H_6 reagents as shown in Figure 1. It is, however, a transition state along the reaction coordinate, having only one imaginary frequency, and a classical energy (i.e., non-zero-point corrected) higher than the separated reagents or separated products (see Table 1). The MP2 results show a strong dependence on the size of the basis set. Both MP2/aug-cc-pVDZ and MP2/aug-cc-pVTZ calculations are within 1 kcal mol^{-1} of the experimental values, but lie on either side of the experimental range, with the larger basis set results predicting a larger exothermicity. The difference between the double- and triple-ζ MP2 reaction energies (∼1.4 kcal mol^{-1}) suggests that MP2 calculations with an infinite basis set will overestimate the reaction exothermicity. The observed agreement between MP2/aug-cc-pVDZ and experimental energy changes seems, therefore, to be a result of a balance of errors emerging from the relatively small size of the basis set and the inability of MP2 calculations to retrieve all of the electronic correlation energy.

Further insight into the effect of electronic correlation on the description of the reaction energy is given by CCSD(T) calculations. The CCSD(T)/aug-cc-pVDZ calculations are in satisfactory agreement with the experiments, but we were unable to determine the dependence upon basis set size as the use of larger basis sets in CCSD(T) geometry optimization was computationally too expensive for our present capabilities. Instead, we determined the dependence of the CCSD(T) reaction

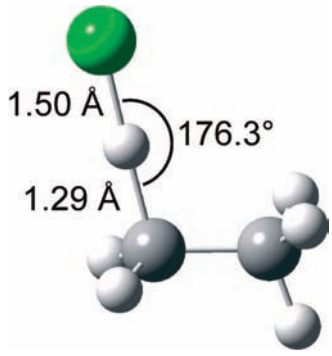

Figure 2. Schematic diagram of the transition-state structure of the $Cl + C_2H_6 \rightarrow HCl + C_2H_5$ reaction, calculated at the MP2/aug-cc-pVTZ level of theory.

energy with basis sets using dual-level calculations. In these calculations, single-point CCSD(T) reaction energy evaluations were carried out with geometries and harmonic frequencies obtained at the MP2/aug-cc-pVTZ level. The legitimacy of these dual-level calculations can be determined by comparing pure CCSD(T)/aug-cc-pVDZ and dual-level CCSD(T)/aug-cc-pVDZ//MP2/aug-cc-pVTZ results. Table 1 shows that the difference between the values provided by these two methods is very small (less than 0.15 kcal mol^{-1} in both the reaction energy and barrier), indicating that the lower-level geometries accurately capture the CCSD(T) values. These dual-level calculations allowed us to estimate the complete basis-set limit (CBS) energies using the two-point extrapolation procedure of Halkier et al.[32] The resultant CCSD(T)/CBS//MP2/aug-cc-pVTZ energy is -3.71 kcal mol^{-1}, which is within $\sim$1 kcal mol^{-1} of the experimental value (-2.11 ± 0.41 kcal mol^{-1} at 298 K[27]) after applying a thermal correction ($\sim$+0.5 kcal mol^{-1}) to the calculations.

It should be noted that a potential source of error in the computed reaction energies may result from the vibrational frequencies used in calculating the zero-point energy correction to the electronic energies. When compared with experimentally derived ZPE values, the CCSD(T)/aug-cc-pVDZ and MP2/aug-cc-pVTZ methods were seen to overestimate the ZPE of ethane[33] by 1.3 and 2.3 kcal mol^{-1}, respectively. As the vibrational frequencies of the ethyl radical are not all known experimentally, a similar comparison is not possible for the radical products, and we thus cannot judge whether the overestimation of vibrational frequencies of ethane is balanced by a similar error for the ethyl radical in calculations of the energy change of reaction.

B. Reaction Barrier and Transition-State Geometry. We have investigated the transition state of the title reaction using the same methods described above for the reaction energy. Table 1 shows the calculated barrier height with respect to reagents. The barrier connects weakly bound complexes in the reagent and product valleys and lies lower in energy than the reagents' asymptote when the zero-point correction is accounted for. The pre- and post-TS reaction complexes primarily arise through dispersion and dipole−quadrupole interactions, respectively, and will be described in detail later. The transition-state structure, as optimized by the MP2/aug-cc-pVTZ method, is represented in Figure 2. Key geometrical parameters of the optimized structures are shown in Table 2 for selected ab initio methods. A slight difference between the transition state of reaction 1 and that of the smaller homologue $Cl + CH_4 \rightarrow HCl + CH_3$ reaction is that the breaking and forming bonds are not perfectly collinear at the transition state in reaction 1. The Cl−H−C angle

TABLE 2: Representative Parameters of the Transition State of the $Cl + C_2H_6 \rightarrow HCl + C_2H_5$ Reaction[a]

	Cl−H−$CH_2CH_3^{\ddagger}$		
	R(H−Cl)/Å	*R*(C−H)/Å	Cl−H−C/deg
MP2/aug-cc-pVDZ	1.504	1.315	176.2
MP2/aug-cc-pVTZ	1.503	1.294	176.3
CCSD/aug-cc-pVDZ	1.491	1.360	176.8
CCSD(T)/aug-cc-pVDZ	1.483	1.373	176.5
SRP-AM1	1.508	1.337	170.5

[a] All of the calculations are based on unrestricted wave functions.

is slightly smaller than 180° because of interactions with the neighboring nonreacting CH_3 moiety, which is absent in the Cl + CH_4 reaction. The zero-point corrected CCSD(T)/CBS//MP2/aug-cc-pVTZ barrier height was calculated to be -2.77 kcal mol^{-1} relative to reagents. Barrier heights cannot be measured directly by experiment but can be estimated from the slope of the Arrhenius plot for rate constants at low temperatures; a value of 0.147 ± 0.026 kcal mol^{-1} was obtained from thermal rate constants in the 177−353 K temperature range.[34] This value is high, when compared with the calculated values reported here, but the experimental result does agree that there is no significant barrier to reaction. The quantitative difference between the experimental activation energy and the calculated reaction barrier can have various origins. First, the calculated value may be susceptible to errors in the determination of ZPEs for such large systems. Second, it should be noted that in estimating the reaction barrier, the zero-point energy correction is calculated for the transition-state structure obtained on the classical (i.e., without including zero-point energy) PES. It is possible that the transition state in the vibrationally adiabatic PES occurs at geometries significantly different than those of the classical PES. Verification of this possible complication would require many harmonic-frequency evaluations along the minimum-energy reaction path, which is prohibitive at this time.

The geometry of the saddle point of reaction 1, calculated at the CCSD/aug-cc-pVDZ level, is very similar to that calculated at the CCSD(T)/aug-cc-pVDZ level (see Table 2), implying that inclusion of the triple excitations may not be very important in determining the optimum TS geometry. On the other hand, neglecting the triple excitations does have consequences for the energetics: CCSD/aug-cc-pVDZ calculations were found to lead to a difference of $\sim$2 kcal/mol in the barrier height when compared with the CCSD(T)/aug-cc-pVDZ results.

C. Post- and Prebarrier Wells. As was noted previously,[9,24] in the Cl + C_2H_6 and Cl + CH_4 reaction systems, the HCl departing from a reactive encounter can interact with the ethyl or methyl radical via a dipole−quadrupole interaction to form a shallow well. Table 3 shows calculated energies for the post barrier complex for the former reaction, and Table 4 contains key geometrical parameters. The geometry of the complex, calculated at the MP2/aug-cc-pVTZ level, is shown in Figure 3.

Even though the potential energy well associated with the reaction complex is relatively shallow, its depth is comparable to the reaction exothermicity and the difference in energy between the transition state and products. Therefore, this well could have a significant impact on the scattering dynamics at low collision energies, at which the system is constrained to travel along regions of the PES around the minimum-energy reaction path. For example, the well might influence the rotational distribution of the HCl products as has been argued in the case of reactions of Cl with polar molecules such as CH_3OH.[4,35] As the geometry of the products' valley well for

TABLE 3: Energy (kcal/mol) of the Products' Valley Minimum in the Cl + C_2H_6 → HCl + C_2H_5 Reaction[a]

	Cl−H···C_2H_5
MP2/aug-cc-pVDZ	−2.97
MP2/aug-cc-pVTZ	−3.42
MP2/aug-cc-pVQZ//MP2/aug-cc-pVTZ	−3.56
CCSD(T)/aug-cc-pVDZ//MP2/aug-cc-pVTZ	−1.86
CCSD(T)/aug-cc-pVTZ//MP2/aug-cc-pVTZ	−3.14
SRP-AM1	−3.18

[a] Energies are referred to products. All of the calculations are based on unrestricted wave functions. Energies are not zero-point corrected. The basis-set superposition error has been removed using the counterpoise method.

TABLE 4: Calculated Geometry of the Products' Valley Minimum in the Cl + C_2H_6 → HCl + C_2H_5 Reaction[a]

	Cl−H···C_2H_5		
	R(H−Cl)/Å	*R*(C−H)/Å	Cl−H−C/deg
MP2/aug-cc-pVDZ	1.306	2.077	172.9
MP2/aug-cc-pVTZ	1.294	2.059	172.7
SRP-AM1	1.311	2.175	152.0

[a] All of the calculations are based on unrestricted wave functions.

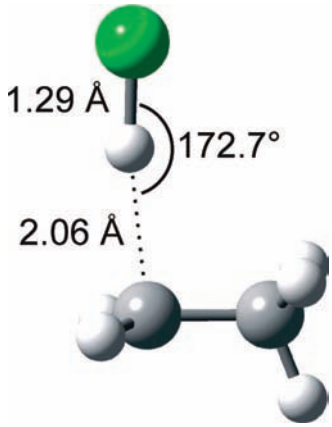

Figure 3. Schematic diagram of the structure corresponding to the product valley minimum in the Cl + C_2H_6 → HCl + C_2H_5 reaction, as calculated at the MP2/aug-cc-pVTZ level of theory.

reaction 1 has only a 4° difference in ∠Cl−H−C angle from the TS (both stationary points are nearly collinear), the well might arrest rotational excitation of the HCl product induced by possible torques during the collision. Experiments indeed measure low rotational excitation in HCl.

We now turn our attention to the shallow minimum in the reactants' valley. To locate the minimum, we scanned the collinear approach of Cl to a H−C bond of ethane in 0.1 Å steps. The scan was performed at the CCSD(T)/aug-cc-pVTZ level of theory, including counterpoise correction of the basis-set superposition error. At that level of theory, the well has a depth of only 0.50 kcal mol^{-1} (with respect to separated reagents) and occurs at a Cl−H separation of 2.7 Å. We also examined the approach of Cl collinearly to the C−C bond (C_{3v} symmetry). The well along this approach is marginally deeper (0.92 kcal mol^{-1}) but still is at relatively long-range, with a Cl−C separation of 3.3 Å. In addition, this well does not occur directly along the reaction coordinate.

The small depth and long-range of this prebarrier well suggest its impact on the dynamics of the title reaction at the energies of most experiments (typically >5 kcal mol^{-1}) will be limited. No pressure dependence of the rate of reaction 1 has been reported, supporting the view that this shallow pre-TS well is not an important contributor to the reaction mechanism at typical collision energies. On the other hand, the well in the post-TS region is considered to be more dynamically significant.

III. Specific Reaction Parameters Semiempirical AM1 Hamiltonian

The prior section described the properties of the main stationary points of the ground-state PES of reaction 1. In this section, we show how ab initio information for the global PES is used to derive a set of parameters for the AM1 semiempirical Hamiltonian[36] specific to reaction 1. Development of specific-reaction-parameters (SRP) semiempirical Hamiltonians was pioneered by Truhlar and co-workers,[37] and has been recently used as a promising technique to produce computationally inexpensive but potentially accurate electronic-structure methods with which to carry out direct-dynamics reactive-scattering simulations.[9,38,39]

Two sets of ab initio data were employed as a benchmark to derive the SRP-AM1 Hamiltonian. First, we used information on all of the stationary points described in section II, including reagents, products, transition state, and products' valley minimum. Second, we calculated reaction paths connecting reagents and products with the transition state. Because our ultimate goal is to simulate the dynamics of the reaction occurring at low energies, we concentrated on the minimum-energy reaction path and approaches in its vicinity. To map the minimum-energy reaction path, we followed the intrinsic reaction coordinate (IRC) from the transition state toward reagents and products. The IRC was calculated at the MP2/aug-cc-pVDZ level, but the energies of the points obtained were then recalculated at the CCSD(T)/aug-cc-pVDZ level. A second reaction pathway that we considered is the collinear approach of Cl to the C−H bond that breaks. Two PES scans were considered for this approach. First, we scanned the C−H bond from 1.35 to 3.80 Å to map the region of the potential energy surface connecting the transition state with products. Second, we scanned the Cl−H bond from 1.50 to 3.00 Å to cover the approach of reagents to the transition state. In these two PES scans, the Cl−H−C angle was held fixed at 180° and the rest of the variables were optimized at the MP2/aug-cc-pVDZ level. The energies of the points obtained in that scan were subsequently recalculated at the CCSD(T)/aug-cc-pVDZ level to obtain a more accurate description of the PES.

This grid of CCSD(T)/aug-cc-pVDZ ab initio points was employed as a reference in the derivation of the SRP-AM1 Hamiltonian. Departing from the original set of AM1 parameters for the Cl, H, and C atoms,[36] we used a nonlinear least-squares procedure to obtain a new set of parameters that minimized the difference between the CCSD(T)/aug-cc-pVDZ and AM1 energies. The resulting SRP-AM1 Hamiltonian notably improves over the results of the standard AM1 method, and the differences between the SRP-AM1 semiempirical and ab initio energies are very small. Figure 4 shows a comparison between SRP-AM1 and ab initio energies in the region of the PES connecting the transition state with products (the Cl−H−C moiety is collinear in the calculations). This is a crucial region of the surface, as it controls the onset of product separation and therefore the partitioning of energy into the various products' degrees of freedom. The SRP-AM1 Hamiltonian reproduces very well the highest-quality energies shown in the figure (CCSD(T)/aug-cc-pVTZ). In fact, Figure 4 shows that the accuracy of the SRP-AM1 Hamiltonian derived in this work is superior to some first-principles techniques, such as MP2 or HF with the large aug-

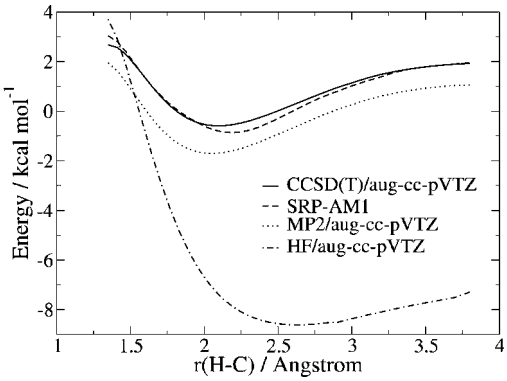

Figure 4. Potential energy surface relaxed scans of the region connecting the transition state and products in the $Cl + C_2H_6 \rightarrow HCl + C_2H_5$ reaction. The Cl−H−C angle was held fixed to 180° during the calculations. All of the first-principles energies correspond to dual-level calculations using geometries calculated at the MP2/aug-cc-pVDZ level. The energies are referenced to a value of zero for the separated reagents.

cc-pVTZ basis set. This is particularly remarkable because the SRP-AM1 electronic-structure method is orders of magnitude faster than any of the first-principles methods.

Tables 1–4 show the properties of the stationary points predicted by the SRP-AM1 Hamiltonian derived in this work in comparison with ab initio methods. The data in Table 1 demonstrate that the reaction energy and barrier of the SRP-AM1 Hamiltonian lie within 1 kcal mol^{-1} of our most accurate CCSD(T) estimates. This makes a large difference compared to the original AM1 Hamiltonian, which shows a deviation of over 20 kcal mol^{-1} from experiment in the reaction energy and does not have a first-order saddle point (the PES is continuously downhill from reagent to products). The transition-state geometry predicted by the SRP-AM1 Hamiltonian is also in agreement with first-principle calculations. In fact, although the SRP-AM1 Cl−H distance is similar to MP2 predictions and is within only 0.025 Å of CCSD(T)/aug-cc-pVDZ results, the H−C distance is actually better described by the SRP-AM1 Hamiltonian than by MP2 methods, when compared with CCSD and CCSD(T) estimates. The major discrepancy between ab initio and SRP-AM1 geometries occurs for the Cl−H−C angle, with the semiempirical predictions showing a deviation of 6° from ab initio predictions. However, this deviation is inconsequential from an energetic point of view because the difference in the system energy with such a slight change in the Cl−H−C angle is very small. For instance, CCSD(T)/aug-cc-pVDZ calculations predict that the energy of the transition state only increases by 0.15 kcal mol^{-1} when going from the minimum-energy Cl−H−C angle (176.5°) to 170°.

The remarkable description of the reaction energetics and transition-state geometry by the SRP-AM1 Hamiltonian is also maintained for the products' valley well, as can be seen in Figure 4. Table 3 shows that the SRP-AM1 Hamiltonian nicely reproduces the well depth predicted by the most accurate ab initio methods explored in this work. The geometry of the minimum is also reasonably captured by the semiempirical estimates (Table 4). The SRP-AM1 bond distances agree well with first-principles calculations. However, the Cl−H−C angle is not in such good agreement, deviating by about 20° from MP2 predictions. Doubtless, this is the largest source of disagreement between the SRP-AM1 Hamiltonian and ab initio calculations. All of our attempts to improve the description of this angle by SRP AM1 Hamiltonians resulted in larger deviations from ab initio predictions in other regions of the PES. The parameters of this SRP AM1 Hamiltonian are shown in Table 5 in comparison with the original set of AM1 parameters.

There has been an earlier attempt at deriving an SRP-AM1 Hamiltonian for the title reaction.[24] A few differences between that prior effort and the work described in this paper are worth noting. First, although the prior SRP Hamiltonian was derived on the basis of information for only the stationary points, in this work we have used extensive CCSD(T)/aug-cc-pVDZ calculations covering not only the stationary points but also regions of the PES connecting them. Second, the level of ab initio theory used in the calculations from which the SRP Hamiltonian was derived in the previous work was restricted to MP2/aug-cc-pVDZ. In this work, even though we have calculated an extensive grid of ab initio points, the level of theory of such calculations has been raised to CCSD(T)/aug-cc-pVDZ. Because the SRP-AM1 Hamiltonian in this work has been derived using a better coverage of the PES at a higher ab initio level than earlier work, it is expected that its accuracy will be superior. In the next section, we show the results of trajectory calculations that have been propagated directly with the SRP-Hamiltonian just described.

IV. Trajectory Study

A. Initial Conditions. The SRP-AM1 Hamiltonian has been used to calculate trajectories with on-the-fly computation of potential energy and forces, and with initial conditions appropriate to the methodology of the experiments of Kandel et al.[15] and subsequent work in our laboratory.[40] In the experiment, chlorine atoms were produced by Cl_2 photodissociation at 355 nm, leading to COM-frame collision energies of ∼5.5 kcal mol^{-1}. The initial conditions of the trajectories were thus fixed so that the Cl atom speed was 1678 m/s. In the experiments, the ethane coreagent was cooled in a molecular beam expansion, and our calculations therefore include only ZPE in the normal modes of this molecule.

At the outset of each trajectory, the position of the ethane molecule relative to the incoming Cl atom was randomized as follows: the ethane (at its equilibrium geometry) had its COM fixed at the origin. The angle of the molecular axis (C−C bond) from the $+z$ axis (θ) was randomly sampled in the range $[0,\pi]$, and the angle from the $+x$ axis (ϕ) and the molecular axis rotation (ψ) were both Monte-Carlo selected independently in the range $[0,2\pi]$.[41] The impact parameter, b, of the incoming Cl atom (which approaches with its relative velocity vector, $\mathbf{v}_{rel}$, parallel to the z-axis, as shown in Figure 5) was linearly randomly sampled between 0 and 4.0 Å. The initial displacement of the Cl atom from the ethane COM was 4.5 Å to ensure the initial interaction energies of the two reagents were negligible, while at the same time allowing the self-consistent field (SCF) energy calculations with the SRP-AM1 Hamiltonian to converge. ZPE was then given to all of the normal modes of ethane (with random phase, and thus random variation of initial atomic positions) as described below.

The Hessian matrix for ethane was computed and diagonalized (at the same SRP-AM1 level of theory used for trajectory propagation) yielding the vibrational mode frequencies and eigenvectors. The ZPE of ethane was included using both uniform and Wigner sampling of the normal modes to determine the effect, if any, of this type of initial conditions sampling. For uniform sampling, random initial displacements (and associated velocities) for each vibrational mode were individually selected from a distribution described by the corresponding ground-state harmonic oscillator wave function.[41] For Wigner sampling, the initial displacements and velocities were instead

TABLE 5: AM1 Original and SRP Parameters That Have Been Modified in This Work for the Cl + C_2H_6 → HCl + C_2H_5 Reaction As Implemented in the GAMESS Code[48]

	H		C		Cl	
	original	SRP	original	SRP	original	SRP
U_{ss}	−11.396427	−11.494465	−52.028658	−54.275537	−111.613948	−120.528986
U_{pp}			−39.614239	−40.095692	−76.640107	−74.045576
ζ_s	1.188078	1.344028	1.808665	1.729372	3.631376	3.611679
ζ_p			1.685116	1.590314	2.076799	2.299980
β_s	−6.173787	−6.516212	−15.715783	−17.357218	−24.594670	−24.333312
β_p			−7.719283	−6.796821	−14.637216	−15.194526
α	2.882324	2.807806	2.648274	2.797891	2.919368	2.823924
G_{ss}	12.848000	13.458449	12.230000	12.654761	15.030000	15.996286
G_{sp}			11.470000	10.321452	13.160000	12.735156
G_{pp}			11.08000	10.744687	11.300000	12.340188
G_{p2}			9.840000	10.326424	9.970000	9.350518
H_{sp}			2.430000	2.484784	2.420000	2.442244

randomly selected according to the Wigner distribution[42] of the corresponding ground-state harmonic oscillator wave function. We note that the Wigner sampling method does not give a constant energy set of initial conditions. Although sampling initial geometries through displacement along rectilinear normal mode coordinates may introduce some total angular momentum, tests showed that this is small ($L \sim 0$) and did not introduce additional rotation.

The treatment of ZPE in classical trajectories must be given careful consideration because the problem of ZPE-leakage can introduce errors. There are two general approaches to solving the ZPE-leakage issue which can be classified as passive and active. The simpler passive approach does not involve any change in the way trajectories are propagated but instead simply rejects trajectories which give energies in one product that are below the ZPE energy value.[43–45] This strategy has the unfortunate consequence of reducing the number of trajectories that can be analyzed, thus increasing computational cost of a QCT study. For the more complicated active approach, the energy in the vibrational modes is monitored during the propagation of the trajectory and corrected if the internal energy content drops below the ZPE level.[46] This correction can cause the trajectory to act unphysically. Here we adopt the more straightforward passive strategy, described in detail below.

B. Running Trajectories. All trajectories were propagated with the dynamic-reaction-coordinate (DRC)[47] function in GAMESS-US[48] using the SRP-AM1 Hamiltonian to calculate the energy gradients along all coordinates at each trajectory time step. Integration of the classical equations of motion was executed with a time step of 0.2 fs, until the termination criteria had been achieved, typically after 2000−3000 steps. A trajectory was deemed to be successfully reactive when the classical rotational angular momentum of the product HCl was stable to better than $\Delta J = 0.001$ between sequential steps and the distance between the Cl and C atoms was at least 7 Å, thereby ensuring that the interaction energy of the products was negligible. Throughout each trajectory, the DRC function ensured that the total energy was conserved to 0.02 kcal mol^{-1} or better. Two sets of trajectories were initiated; one for uniform normal mode sampling, and one for the Wigner normal mode sampling method described above.

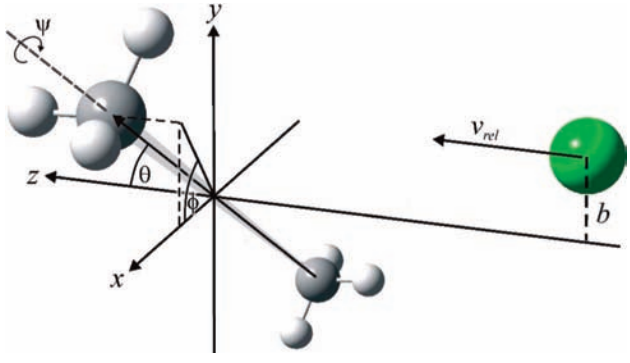

Figure 5. Initial conditions for a trajectory with the incoming Cl atom velocity vector and ethane orientation angles highlighted. The ethane COM is located at the origin and *b* is the impact parameter.

C. Analysis of Trajectories. Trajectories were analyzed using the coordinates and COM velocity vectors provided by the DRC function to give observables that can be compared directly with experimental data. The scattering angle of a trajectory was determined from the final HCl, and initial Cl velocity vectors. The translational energies (E_T) of the HCl and radical products were calculated from the COM velocity of each. The internal (rotational and vibrational) energies of both products were established via the following methodology: J_{HCl} and J_R were calculated from the instantaneous coordinates and velocity vectors of the constituent atoms, classical quantization was achieved by rounding to the nearest integer value. The HCl vibrational energy was treated as the sum of kinetic and potential energy contributions: the kinetic energy was derived by resolving the component of the velocity vectors of both atoms along the H−Cl internuclear axis. To obtain the potential energy contribution to the vibrational energy at any internuclear separation a potential energy curve was computed for isolated HCl at the same SRP-AM1 level of theory used to propagate the trajectories and fitted to a cubic spline function. The vibrational energy of the radical fragment was then determined through energy conservation.

D. Product Energy Distributions. A total of 10000 trajectories were initiated for both the uniform and Wigner methods of normal mode sampling. Approximately one-third of the trajectories were reactive, with a complete trajectory taking, on average, 4−5 min of CPU time. Trajectory analysis was carried out using the procedures outlined in part C. Figure 6 shows the computed rotational distributions of HCl products for both uniform and Wigner sampling of initial conditions, and in both cases the distribution is hotter than experimentally determined.[49] This effect has been seen previously in QCT calculations of Cl + RH (R = alkyl) and Cl + CH_3OH initiated at the TS,[26] which demonstrated that ZPE in RH bends in the TS broadens the rotational distribution via bending-rotation coupling.[9] Indeed, the use of classical mechanics places no restrictions on the flow of energy in the reactive system, allowing such bending-rotation

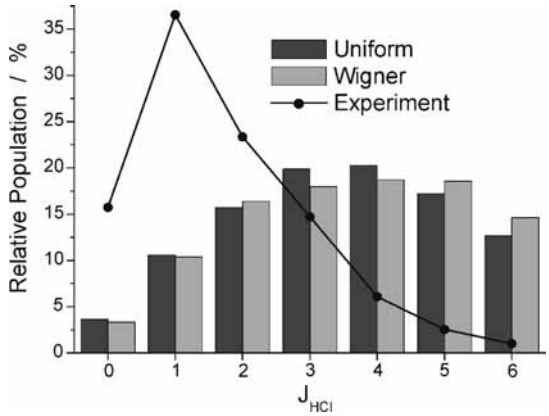

Figure 6. Rotational distribution of HCl products after removal of reactive trajectories that violated ZPE conservation as described in the main text. The computational outcomes for uniform (dark gray boxes) and Wigner (light gray boxes) sampling of initial conditions are compared with experimental results (●).

and vibration-translation couplings to occur. In the current calculations, many ethyl product molecules are formed with energies well below their zero point level; the extra energy can be channeled into other available modes, such as HCl rotation and product relative translation. To counteract such effects, we employed passive ZPE leakage correction,[43–45] and only considered reactive trajectories with $J_{HCl} < 6$ [the highest experimentally observed rotational state] and $E_{vib}(R) > 37.1$ kcal mol^{-1} [which is 1 kcal mol^{-1} below the calculated ethyl radical ZPE]. These constraints on acceptable outcomes left only 1319 (Wigner-sampling initiated) and 1208 (uniform-sampling initiated) trajectories to analyze (i.e., <40% of reactive trajectories satisfied the criteria imposed for ZPE and maximum HCl rotation). Constraining the upper limit of J_{HCl} had little effect on the computed distributions of product KE release and scattering angles but is consistent with the comparisons drawn below with experimental measurements made for HCl in low rotational levels.

It is worth noting that there are inherent problems when trying to describe correctly HCl rotation, when this degree of freedom of the products only receives a small fraction (~0.2 kcal mol^{-1}) of the total energy available, yet the expected accuracy of the PES is no better than 1 kcal mol^{-1}. Although the deviation between most populated J_{HCl} levels for experiment and theory corresponds to three quanta, the absolute differences in energy for J_{HCl}=1 and 4 amounts to only ~0.5 kcal mol^{-1} and thus might still be below expectations of "chemical accuracy" (i.e., within 1 kcal mol^{-1}).

Trajectories were examined for evidence of chattering type behavior,[25] and only a small fraction (<3%) of such trajectories were found. This is in contrast to our previous trajectory study where, by carefully constraining the orientations of the reagents and their impact parameters we observed 16% of trajectories to proceed via a chattering mechanism.[25] Chattering is associated with an H-atom motion between the heavier Cl and C atoms that involves recrossing of the TS; it is thus not thought to be a feature of the shallow collinear well prior to the TS, for which the Cl−C distance is computed (at the CCSD(T)/aug-cc-pVTZ level) to be 3.8 Å and the H atom would need to undergo very large (~1.4 Å) motion to recross the reaction energy barrier. The products of chattering trajectories in the current calculations were distributed in HCl rotational quantum state, internal energy of the ethyl radical and E_T in much the same way as those from nonchattering trajectories, suggesting no significant effect of

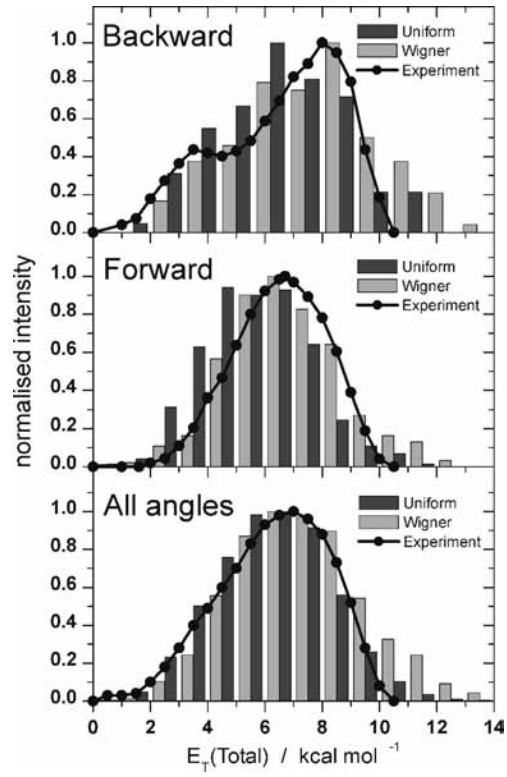

Figure 7. Distribution of total translational energy (E_T(total)) release for forward (top panel, scattering angle < 60°) and backward (middle panel, scattering angle > 120°) scattered trajectories in comparison with experimental data from Huang et al.[21] (at the higher collision energy of 6.7 kcal mol^{-1}). The bottom panel shows the results summed over all scattering angles. Note the absence of the slow products' peak in the backward scattered distribution that was attributed to chattering collisions in the experiment. Dark and light gray boxes indicate, respectively, uniform and Wigner sampling of trajectory initial conditions; experimental results are denoted by ●.

chattering on product energies (within the limitation of our classical trajectories). Owing to the small number of computed chattering trajectories, however, any further analysis of this unusual mechanism was not possible.

Figure 7 shows a comparison between calculated and experimental E_T distributions for backward (scattering angle > 120°) and forward (scattering angle < 60°) scattered trajectories, and for trajectories summed over all scattering angles, with the angular ranges and experimental data taken from the CMB experiments of Haung et al.[21] The satisfactory computational simulation of all the data sets, with nearly quantitative reproduction of the distribution widths and maxima of the experimental results, is very encouraging. We do not, however, see any evidence of the bimodal structure in the backward scattered E_T distribution that was experimentally observed by Huang et al.,[21] which may be a consequence of ZPE leakage from the ethyl product internal modes obscuring the fine structure in the kinetic energy release distributions. The 1 kcal mol^{-1} tolerance placed on the leakage of ZPE, and errors in the computed energy change for the reaction (using the SRP-AM1 Hamiltonian) are responsible for calculation of products with a higher total translational energy than is observed in the experiments. Interestingly, the results obtained with Wigner sampling of the initial conditions for ethane agree better with experiment than those obtained with uniform sampling.

E. Angular Distributions. In Figure 8 we present the first computed DCS for products of the Cl + ethane reaction generated using all degrees of freedom on a fully dimensional

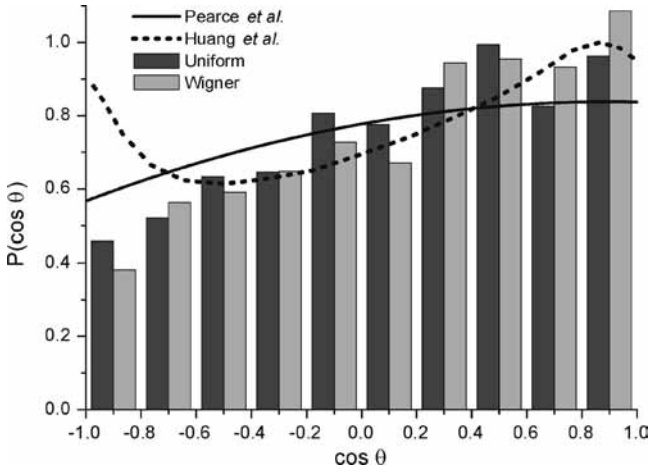

Figure 8. Comparison of calculated scattering distributions for HCl(J=0−6) for a mean collision energy of 5.4 kcal mol^{-1}, and experimentally determined DCSs for HCl(v=0,J=1). The solid line is experimental data from ref 40 at $\langle E_{coll} \rangle$ = 5.4 kcal mol^{-1}; the dashed line is the result of the CMB experiments of Suits and co-workers at $\langle E_{coll} \rangle$ = 6.7 kcal mol^{-1}. Dark and light gray boxes indicate, respectively, uniform and Wigner sampling of trajectory initial conditions.

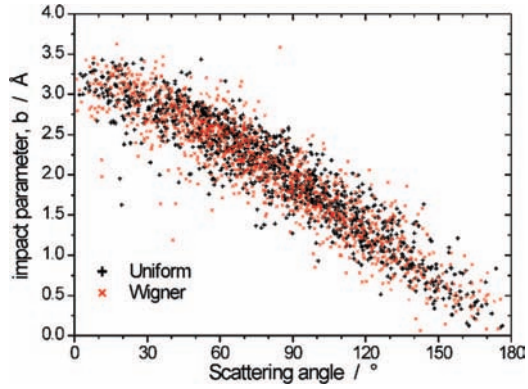

Figure 9. Correlation between the impact parameter of the incoming Cl atom and the COM frame scattering angle of the HCl product.

PES. The figure compares our calculated DCS with the experimental results of Pearce et al.[40] and, at a higher collision energy, Huang et al.[21] The reduction in the number of successful trajectories resulting from the passive ZPE leakage correction means it was not possible to calculate state resolved DCSs for individual rotational levels of HCl. Figure 8 thus shows a quantum-state averaged DCS for HCl(v=0,J=0−6). The computed distribution compares favorably with the experimental results, showing broad angular scattering with a small preference for forward scatter. The choice of sampling method for initial conditions (Wigner versus uniform) has no significant effect on the outcomes. A possible reason for the poorer agreement in the backward scattered region is the need for exclusion of more backward scattered trajectories because a greater number violated the threshold criterion for ZPE in the C_2H_5 radical.

Analysis of trajectories allowed us to compare computed scattering angles with the initial impact parameters of the collision (defined relative to the COM of the ethane molecule as shown in Figure 5). Figure 9 shows that the scattering angle of the HCl product is strongly influenced by the impact parameter of the collision, with large b resulting in small values of θ, and small b giving large scattering angles. For the trajectories shown here, sampling of b was limited to a maximum value, b_{max} = 4.0 Å. A simple hard-sphere model of the scattering[50] predicts that cos θ depends linearly on b^2 but such a dependence is not observed. No further correlations were found between the initial conditions and observables of the trajectories.

V. Conclusions

A fully dimensional quasiclassical trajectory calculation study of the reaction of Cl atoms with ethane, employing a reparameterized AM1 Hamiltonian to provide an accurate description of the potential energies in the vicinity of the reaction path, has generated outcomes that can be compared to a variety of experimental measurements on this important reaction. The standard AM1 Hamiltonian was greatly improved for our purposes by reoptimization of the parameters by fitting to a grid of CCSD(T)/aug-cc-pVDZ ab initio calculations covering critical regions of the potential energy surface. The resultant semiempirical SRP-AM1 Hamiltonian made on-the-fly calculation of potential energy points along a trajectory sufficiently fast for us to calculate 20000 fully dimensional quasi-classical trajectories. Two methods (uniform and Wigner) for initial sampling of the normal modes of vibration of the ethane reactant were used. Computed kinetic energy release and COM frame angular scattering distributions show satisfactory agreement with the experimental data, lending support to the quality of the potential energy function employed for the QCT calculations. The choice of sampling method had no great effect on the observable outcomes of the trajectories (the only observed difference being in the E_T distributions). A remaining limitation of the method is the effect of leakage of zero point energy from the many vibrational modes of the reacting species. This well-known drawback of the QCT approach can result in violation of the quantum mechanical restrictions that are present in experimental studies of translational and internal energies. In the current study, a simple correction by rejection of nonphysical trajectories was employed but resulted in a significant reduction in the efficiency of completion of trajectories.

Acknowledgment. This work has been supported by the EPSRC LASER Portfolio Partnership grant GR/S71750/01. A.J.O.E. thanks the Royal Society and the Wolfson Foundation for a Research Merit Award. D.T. thanks the National Science Foundation under Grant No. 0547543 and AFOSR under Grant No. FA9550-06-1-0165. D.T. is a Cottrell Scholar of Research Corporation. The authors are also grateful to Prof. J. N. Harvey for his assistance with the trajectory calculations, and R. A. Rose, J. K. Pearce and B. Retail for many helpful discussions.

References and Notes

(1) Ausfelder, F.; McKendrick, K. G. *Prog. Reaction Kinet. Mech.* **2000**, *25*, 299–370.
(2) Whitney, E. S.; Zolot, A. M.; McCoy, A. B.; Francisco, J. S.; Nesbitt, D. J. *J. Chem. Phys.* **2005**, 122. 124310/1−124310/10.
(3) Liu, K. *Phys. Chem. Chem. Phys.* **2007**, *9*, 17–30.
(4) Murray, C.; Orr-Ewing, A. J. *Int. Rev. Phys. Chem.* **2004**, *23*, 435–482.
(5) Simpson, W. R.; Orr-Ewing, A. J.; Zare, R. N. *Chem. Phys. Lett.* **1993**, *212*, 163–171.
(6) Simpson, W. R.; Orr-Ewing, A. J.; Rakitzis, T. P.; Kandel, S. A.; Zare, R. N. *J. Chem. Phys.* **1995**, *103*, 7299–7312.
(7) Simpson, W. R.; Rakitzis, T. P.; Kandel, S. A.; Orr-Ewing, A. J.; Zare, R. N. *J. Chem. Phys.* **1995**, *103*, 7313–7335.
(8) Simpson, W. R.; Rakitzis, T. P.; Kandel, S. A.; Lev-On, T.; Zare, R. N. *J. Phys. Chem.* **1996**, *100*, 7938–7947.
(9) Troya, D.; Weiss, P. J.E. *J. Chem. Phys.* **2006**, 124. 074313/1−074313/12.
(10) Zhang, B.; Liu, K. *J. Chem. Phys.* **2005**, *122*, 101102/1–101102/4.
(11) Retail, B.; Pearce, J. K.; Murray, C.; Orr-Ewing, A. J. *J. Chem. Phys.* **2005**, 101101/1–101101/4.
(12) Retail, B.; Greaves, S. J.; Pearce, J. K.; Rose, R. A.; Orr-Ewing, A. J. *Phys. Chem. Chem. Phys.* **2007**, *9*, 3261–3267.

(13) Zhang, L. L.; Lu, Y. P.; Lee, S. Y.; Zhang, D. H. *J. Chem. Phys.* **2007**, 127. 234313/1−234313/7.

(14) Murray, C.; Pearce, J. K.; Rudić, S.; Retail, B.; Orr-Ewing, A. J. *J. Phys. Chem. A* **2005**, *109*, 11093–11102.

(15) Kandel, S. A.; Rakitzis, T. P.; Lev-On, T.; Zare, R. N. *J. Chem. Phys.* **1996**, *105*, 7550–7559.

(16) Rakitzis, T. P.; Kandel, S. A.; Lev-On, T.; Zare, R. N. *J. Chem. Phys.* **1997**, *107*, 9392–9405.

(17) Kandel, S. A.; Rakitzis, T. P.; Lev-On, T.; Zare, R. N. *J. Phys. Chem. A* **1998**, *102*, 2270–2273.

(18) Samartzis, P. C.; Smith, D. J.; Rakitzis, T. P.; Kitsopoulos, T. N. *Chem. Phys. Lett.* **2000**, *324*, 337–343.

(19) Toomes, R. L.; Kitsopoulos, T. N. *Phys. Chem. Chem. Phys.* **2003**, *5*, 2481–2483.

(20) Bass, M. J.; Brouard, M.; Vallance, C.; Kitsopoulos, T. N.; Samartzis, P. C.; Toomes, R. L. *J. Chem. Phys.* **2003**, *119*, 7168–7178.

(21) Huang, C.; Li, W.; Suits, A. G. *J. Chem. Phys.* **2006**, 125. 133107/1−133107/9.

(22) Li, W.; Huang, C.; Patel, M.; Wilson, D.; Suits, A. G. *J. Chem. Phys.* **2006**, 124. 011102/1−011102/4.

(23) Roberto-Neto, O.; Machado, F. B. C. *J. Mol. Struct. (THEOCHEM)* **2002**, *580*, 161–170.

(24) Fernández-Ramos, A.; Martínez-Núñez, E.; Marques, J. M. C.; Vázquez, S. A. *J. Chem. Phys.* **2003**, *118*, 6280–6288.

(25) Greaves, S. J.; Kim, J.; Orr-Ewing, A. J.; Troya, D. *Chem. Phys. Lett.* **2007**, *441*, 171–175.

(26) Rudić, S.; Murray, C.; Harvey, J. N.; Orr-Ewing, A. J. *J. Chem. Phys.* **2004**, *120*, 186–198.

(27) Sander, S. P.; Friedl, R. R.; Ravishankara, A. R.; Golden, D. M.; Kolb, C. E.; Kurylo, M. J.; Huie, R. E.; Orkin, V. L.; Molina, M. J.; Moortgat, G. K.; Finlayson-Pitts, B. J. *Jet Propulsion Laboratory publication 02-25*, JPL: Pasadena, CA, 2003.

(28) Dunning, T. H., Jr. *J. Chem. Phys.* **1989**, *90*, 1007–1023.

(29) Kendall, R. A.; Dunning, T. H., Jr.; Harrison, R. J. *J. Chem. Phys.* **1992**, *96*, 6796–6806.

(30) Frisch, M. J.; Trucks, G. W.; Schlegel, H. B.; Scuseria, G. E.; Robb, M. A.; Cheeseman, J. R.; Montgomery, J. A., Jr.; Vreven, T.; Kudin, K. N.; Burant, J. C.; Millam, J. M.; Iyengar, S. S.; Tomasi, J.; Barone, V.; Mennucci, B.; Cossi, M.; Scalmani, G.; Rega, N.; Petersson, G. A.; Nakatsuji, H.; Hada, M.; Ehara, M.; Toyota, K.; Fukuda, R.; Hasegawa, J.; Ishida, M.; Nakajima, T.; Honda, Y.; Kitao, O.; Nakai, H.; Klene, M.; Li, X.; Knox, J. E.; Hratchian, H. P.; Cross, J. B.; Bakken, V.; Adamo, C.; Jaramillo, J.; Gomperts, R.; Stratmann, R. E.; Yazyev, O.; Austin, A. J.; Cammi, R.; Pomelli, C.; Ochterski, J. W.; Ayala, P. Y.; Morokuma, K.; Voth, G. A.; Salvador, P.; Dannenberg, J. J.; Zakrzewski, V. G.; Dapprich, S.; Daniels, A. D.; Strain, M. C.; Farkas, O.; Malick, D. K.; Rabuck, A. D.; Raghavachari, K.; Foresman, J. B.; Ortiz, J. V.; Cui, Q.; Baboul, A. G.; Clifford, S.; Cioslowski, J.; Stefanov, B. B.; Liu, G.; Liashenko, A.; Piskorz, P.; Komaromi, I.; Martin, R. L.; Fox, D. J.; Keith, T.; Al-Laham, M. A.; Peng, C. Y.; Nanayakkara, A.; Challacombe, M.; Gill, P. M. W.; Johnson, B.; Chen, W.; Wong, M. W.; Gonzalez, C.; Pople, J. A. *Gaussian 03*, revision B.04; Gaussian Inc.: Pittsburgh, PA, 2003.

(31) Amos, R. D.; Bernhardsson, A.; Berning, A.; Celani, P.; Cooper, D. L.; Deegan, M. J. O.; Dobbyn, A. J.; Eckert, F.; Hampel, C.; Hetzer, G.; Knowles, P. J.; Korona, T.; Lindh, R.; Lloyd, A. W.; McNicholas, S. J.; Manby, F. R.; Meyer, W.; Mura, M. E.; Nicklass, A.; Palmieri, P.; Pitzer, R.; Rauhut, G.; Schütz , M.; Schumann, U.; Stoll, H.; Stone, A. J.; Tarroni, R.; Thorsteinsson, T.; Werner, H.-J. *MOLPRO 2002. 6, a package of ab initio programs*; Werner, H.-J., Knowles, P. J., designers; Universität Stuttgart and Cardiff University, Germany and Cardiff, U.K., 2006; http://www.molpro.net.

(32) Halkier, A.; Helgaker, T.; Jørgensen, P.; Klopper, W.; Koch, H.; Olsen, J.; Wilson, A. K. *Chem. Phys. Lett.* **1998**, *286*, 243–252.

(33) Computational Chemistry Comparison and Benchmark Database, IV.C.1 Vibrational Frequency Comparison [Online], NIST Standard Reference Database Number 101; National Institute of Standards and Technology: Gaithersburg, MD, 2005 http://srdata.nist.gov/cccbdb (Release 14, September 2006).

(34) Hickson, K. M.; Keyser, L. F. J. *Phys. Chem. A* **2004**, *108*, 1150–1159.

(35) Murray, C.; Pearce, J. K.; Rudić, S.; Retail, B.; Orr-Ewing, A. J. *J. Phys. Chem. A* **2005**, *109*, 11093–11102.

(36) Dewar, M. J. S.; Zoebisch, E. G.; Healy, E. F.; Stewart, J. J. P. *J. Am. Chem. Soc.* **1985**, *107*, 3902–3909.

(37) Gonzalez-Lafont, A.; Truong, T. N.; Truhlar, D. G. *J. Phys. Chem.* **1991**, *95*, 4618–4627.

(38) Troya, D.; García-Molina, E. *J. Phys. Chem. A* **2005**, *109*, 3015–3023.

(39) Troya, D. *J. Chem. Phys.* **2006**, 123. 214305/1−214305/11.

(40) Pearce, J. K.; Retail, B.; Greaves, S. J.; Rose, R. A.; Orr-Ewing, A. J. *J. Phys. Chem. A* **2007**, *111*, 13296–13304.

(41) Atkins, P. W.; Friedman, R. S. *Molecular Quantum Mechanics*, 3rd ed; Oxford University Press: Oxford, U.K., 1996.

(42) Schinke, R. *Photodissociation Dynamics*; Cambridge University Press: Cambridge, U.K., 1993; Chapter 5, and references therein.

(43) Bradley, K. S.; Schatz, G. C. *J. Chem. Phys.* **1998**, *108*, 7994–8003.

(44) Varandas, A. J. C. *Chem. Phys. Lett.* **2007**, *439*, 386–392.

(45) Espinosa-García, J. *J. Phys. Chem. A* **2007**, *111*, 3497–3501.

(46) Xie, Z.; Bowman, J. M. *J. Phys. Chem. A* **2006**, *110*, 5446–5449.

(47) Schmidt, M. W.; Gordon, M. S.; Dupuis, M. *J. Am. Chem. Soc.* **1985**, *107*, 2585–2589.

(48) Schmidt, M. W.; Baldridge, K. K.; Boatz, J. A.; Elbert, S. T.; Gordon, M. S.; Jensen, J. H.; Koseki, S.; Matsunaga, N.; Nguyen, K. A.; Su, S. J.; Windus, T. L.; Dupuis, M.; Montgomery, J. A. *J. Comput. Chem.* **1993**, *14*, 1347–1363.

(49) Rudić, S.; Murray, C.; Ascenzi, D.; Anderson, H.; Harvey, J. N.; Orr-Ewing, A. J. *J. Chem. Phys.* **2002**, *117*, 5692–5706.

(50) Camden, J. P.; Bechtel, H. A.; Ankeny Brown, D. J.; Martin, M. R.; Zare, R. N.; Hu, W.; Lendvay, G.; Troya, D.; Schatz, G. C. *J. Am. Chem. Soc.* **2005**, *127*, 11898–11899.

(51) IUPAC Subcommittee on Gas Kinetic Data Evaluation, Data Sheet X_VOC5 [Online], http://www.iupac-kinetic.ch.cam.ac.uk/ (updated: 9th August 2002).

JP802347V